RSC Mechanochemistry

ROYAL SOCIETY OF CHEMISTRY

PAPER

View Article Online
View Journal | View Issue

Cite this: *RSC Mechanochem.*, 2025, **2**, 100

Coordination polymers containing dimeric Cu_2X_2 and polymeric $(CuI)_n$ clusters linked by unsymmetrical isomeric pyridine-benzimidazole linkers: modulating photophysical properties by mechanical stimuli†

Prantik Dutta, Abhijit Garai and Kumar Biradha *

Two rigid unsymmetrical linkers, **4-PBI** and **3-PBI**, have been successfully employed to synthesize three CuX cluster-based coordination polymers (CPs). The complexation reaction of **4-PBI** with CuI and CuBr resulted in isostructural crystalline **CP1** and **CP2**, respectively, containing Cu_2X_2 clusters. On the other hand, the isomeric **3-PBI** with CuI resulted in crystalline **CP3** containing a one-dimensional polymeric $(CuI)_n$ cluster. Furthermore, the mechanochromism of the CPs has been examined using DRS, solid state PL, FT-IR and Raman spectroscopy. **CP1** and **CP2** exhibited mechanochromism as their colours changed from reddish brown to orangish yellow upon grinding. The pressure induced local distortion around the flexible dimeric cores of **CP1** and **CP2** was responsible for the resultant mechanochromism. The presence of a polymeric CuI cluster with μ_3-bridging I atoms within the 2D layer of **CP3** renders it rigid, thereby hampering its ability to display mechanochromism.

Received 5th July 2024
Accepted 4th November 2024

DOI: 10.1039/d4mr00071d

rsc.li/RSCMechanochem

Introduction

Coordination complexes and polymers of Cu(I) halides are well known for their exciting photophysical properties given their structural diversity.[1–6] Their versatility and low cost make them an exciting area of research in the field of material science and technology.[7] In particular, the luminescent properties[7–9] of these materials have been used to create functional materials with potential applications such as optoelectronics,[10–12] sensors,[1,6,13,14] storage devices,[15,16] photocatalysts,[17] and heterogeneous catalysts.[18] The diversity in the structures arises from the exhibition of oligomeric CuX clusters, which act as secondary building units (SBUs) for coordination with *exo*-bidentate ligands containing N, P, S and O donors.[19] A CSD search for $(CuX)_n$ cluster-based complexes and CPs reveals 2757 entries, which include dimeric, trimeric, tetrameric and 1D double chain polymeric $(CuX)_n$ clusters. Out of these 2757 entries, 2019 entries (73%) contain Cu_2X_2 (with X = I, Br and Cl representing 1184, 533 and 302 entries, respectively), 51 entries (2%) contain Cu_3X_3 (with X = I, Br and Cl representing 27, 13 and 11 entries, respectively), 477 entries (17%) contain Cu_4X_4 (with X = I, Br and Cl representing 399, 43 and 35 entries, respectively) and 210 entries (8%) contain $(CuX)_n$ double chains (with X = I, Br and Cl representing 98, 52 and 60 entries, respectively). Indeed, the most frequently occurring SBUs of CuX are Cu_2X_2 (rhomboidal) and Cu_4X_4 (cubic), which have potential to form 1D, 2D and 3D framework structures with organic linkers.[20–27] The CSD search indicates that the trimeric $(CuX)_3$ [28,29] and polymeric $(CuX)_n$[30] clusters are relatively less explored SBUs.[31] Moreover, there are other types of $(CuX)_n$ clusters or Cu_mI_n ($m \neq n$) clusters, which are excluded from our search.[19,31,32] In the $(CuX)_n$ containing CPs, the dimensionality of the networks is not only dependent on the geometry of the CuX SBUs, but also heavily dependent on the nature of the linker, the flexibility of the linker, the solvent of crystallization, metal-to-ligand ratios, temperature and the synthetic methodologies.[13,33,34]

The tunable photophysical properties of Cu(I) cluster-based CPs make them an intriguing option for designing smart materials.[35] These CPs exhibit characteristic emission bands that stem from one or more of the following possible triplet states: metal-to-ligand charge transfer (^{3}MLCT), halide-to-ligand charge transfer (^{3}XLCT), halide-to-metal charge transfer (^{3}XMCT) and cluster-centered (^{3}CC). Consequently, the clusters are vulnerable to any external stimuli that could affect the Cu–donor, Cu–X bond length or Cu···Cu interactions associated with the cluster environment.[7] Indeed, applying external stimuli

Department of Chemistry, Indian Institute of Technology Kharagpur, 721302 Kharagpur, India. E-mail: kbiradha@chem.iitkgp.ac.in; Fax: +91-3222-282252; Tel: +91-3222-283346

† Electronic supplementary information (ESI) available: Additional figures for ^{1}H NMR spectra, crystal structure of the CPs, crystallographic information, bond lengths, bond angles, hydrogen bonding parameters, PXRD patterns, FT-IR, TGA, solid state PL, excitation spectra and CIE chromaticity diagram. CCDC 2341925–2341927. For ESI and crystallographic data in CIF or other electronic format see DOI: https://doi.org/10.1039/d4mr00071d

such as heat, mechanical force, or guest vapour results in a subtle change in the HOMO–LUMO gap, which can be observed as a change in the colour or luminescence of the CPs.[36–38] This broad phenomenon is termed 'chromism' and depending on the external stimuli used, the type of chromism is named.

The most commonly found chromism is thermochromism, which was first observed in a $Cu_4I_4py_4$ complex by Hardt and Pierre.[39] On the other hand, mechanochromism, which was first observed by Francis Bacon,[40] has been explored in several materials including organic dyes,[41–43] metal–organic complexes and CPs.[44–48] Recently, Perruchas, Hong, and others have reported mechanochromic CPs containing $(CuI)_n$ clusters coordinated with N, P, and S soft donor ligands.[49–54] Further, Amo-Ochoa and co-workers have reported several thermo- and mechano-responsive 1D CPs containing (CuI) double chains or ladder-like clusters coordinated with the ligands 2-aminopyrazine, 2-amino-4-chloropyrimidine, methyl isonicotinate and methyl 2-aminoisonicotinate.[55–57] The mechanochromic behavior was also observed in CPs containing 0D clusters of $(CuX)_n$.[51,58,59] For example, Bhoomishankar and co-workers reported two hexameric Cu_6I_6 cluster-based multistimuli responsive CPs containing a symmetrical tripodal ligand.[58] Both CPs were shown to exhibit distinct luminescence properties when stimulated thermally and mechanically. Moreover, the dimensionality and the rigidity of CPs were found to play an important role in the stimuli responsiveness of CPs as reported by Harvey and co-workers. In their study, it was demonstrated that a 3D-CP containing Cu_8I_8 cluster exhibits thermochromism but not mechanochromism, attributed to the robust nature of the framework.[59] Recently, Cu_2I_2 dimer containing CPs were shown to exhibit variation in the luminescence properties due to the pressure induced local distortion of the structure around the dimeric core.[60,61]

In continuation of our studies on $(CuX)_n$ cluster-based CPs,[62–65] in this contribution the CuX CPs of rigid unsymmetrical isomeric linkers **4-PBI** and **3-PBI** (Scheme 1) and their mechanochromism properties were explored. Although there are several studies on the mechanochromism of CuI containing CPs, the mechanochromic properties of CuBr containing CPs have not been explored to date. Remarkably, **4-PBI** was found to form two isostructural 2D CPs with CuI and CuBr containing Cu_2X_2 clusters providing a unique opportunity to study the mechanochromism of both the CPs and understand the differences between CuBr and CuI clusters. Further, **3-PBI** was found to form 1D double chain CuI cluster-based CP (**CP3**). The crystal structures are analyzed in detail and the mechano-responsiveness of the CPs was studied extensively. When subjected to mechanical stress, **CP1** and **CP2** were found to exhibit a distinguishable color change, which was investigated with PXRD, FT-IR and Raman spectroscopy. Our research on these CPs paves the way for the synthesis of functional materials with varying structural features, which exhibit different photophysical properties and mechano-responsive behaviour due to the unique $(CuX)_n$ cluster unit they contain.

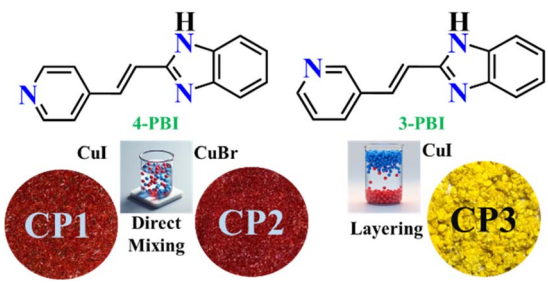

Scheme 1 Formation of CPs from two isomeric linkers and CuX.

Results and discussion

The ligands **4-PBI** and **3-PBI** were synthesized using a condensation reaction of *o*-phenylenediamine with 4-pyridylacrylic acid (4-PAA) and 3-pyridylacrylic acid (3-PAA), respectively. The complexation reaction of **4-PBI** with CuI and CuBr in acetonitrile (ACN) resulted in the single crystals of $\{[CuI(\textbf{4-PBI})]\cdot(ACN)\}_n$, **CP1** and $\{[CuBr(\textbf{4-PBI})]\cdot(ACN)\}_n$, **CP2**, respectively. However, similar reactions of **3-PBI** with CuI or CuBr did not result in any single crystals despite several trails. Notably, the single crystals of $\{[Cu_2I_2(\textbf{3-PBI})]\cdot(DMF)\}_n$, **CP3** were obtained through slow diffusion of ACN solution of CuI into DMF solution of **3-PBI**. However, the same process in the case of the **3-PBI** reaction with CuBr did not yield suitable single crystals for diffraction. Pertinent information including crystallographic parameters, bond lengths, bond angles and intermolecular interactions for **CP1–3** is given in the ESI (Tables S1–3, ESI).† Both **CP1** and **CP2** crystallize in the monoclinic space group *C*2/*c* and are found to be isostructural. The asymmetric units contain one unit each of the ligand, Cu(I) ion, halide ion and ACN molecule (Fig. S2a, ESI†). In both structures, the halide ions I^- or Br^- exhibit μ_2-bridging and form Cu_2X_2 units, which act as planar four connecting SBUs. The SBUs are found to be unsymmetrical as they are composed of two long and two short distances: Cu–I distances are 2.6501(5) and 2.7072(6) Å in **CP1** and Cu–Br distances are 2.5250(5) and 2.6084(6) Å in **CP2**. The Cu···Cu distances within the SBUs are 2.9708(5) and 3.0917(6) Å in **CP1** and **CP2**, respectively. In both the CPs, each SBU is connected with four ligands—two of them are through imidazole N-atom coordination and the rest are through pyridyl N-atoms (Fig. 1a). As each ligand can connect two SBUs, it leads to the formation of a two-dimensional network with corrugated geometry (Fig. 1b). Within the layer, the N–H groups of imidazole units form N–H···I (N···I, ∠N–H···I: 3.478(2) Å, 129°) and N–H···Br interactions (N···Br, ∠N–H···Br: 3.3336(18) Å, 152°, Fig. S2b, ESI†). The solvent ACN was incorporated in between the layers *via* weak C–H(ACN)···X interactions (C···I, ∠C–H···I: 3.839(3) Å, 130° in **CP1** and C···Br, ∠C–H···Br: 3.741(3) Å, 144° in **CP2**) as shown in Fig. 1c.

CP3 crystallizes in the $Pna2_1$ space group with an asymmetric unit containing one **3-PBI**, two Cu(I) ions, two I^- ions and one DMF (Fig. S2c, ESI†). Each Cu(I) centre is connected to three μ_3-bridging I^- ions and one linker in a distorted tetrahedral fashion forming a one dimensional double chain or a ladder of $(CuI)_n$ clusters along the *b*-axis (Fig. 1d) with Cu–I distances of

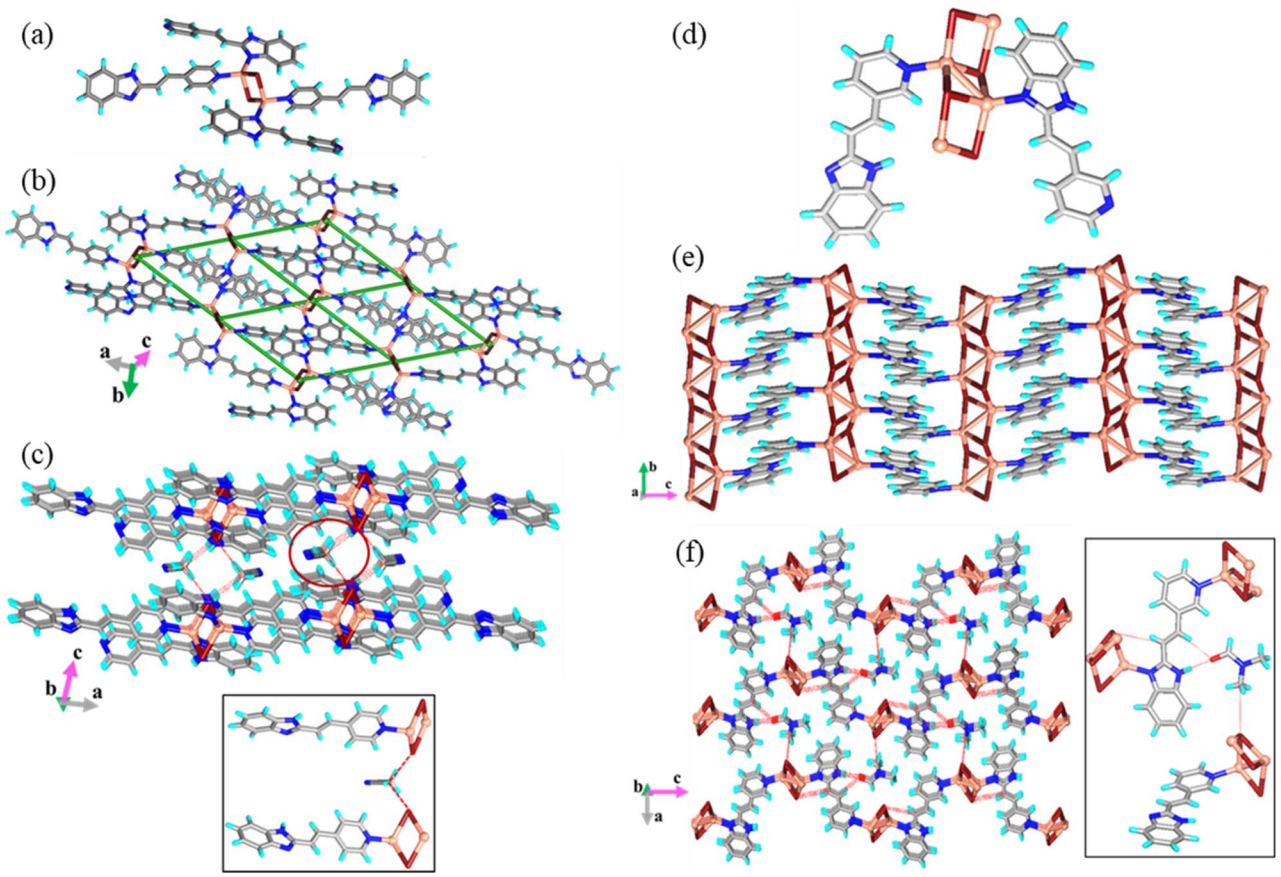

Fig. 1 Illustrations for the crystal structures of **CP1** and **CP2**: (a) Cu_2X_2 rhomboid dimer and the coordination environment of **CP2**; (b) 2D grid type of network in the *ab*-plane; (c) stacking of 2D layers along the *c*-axis, notice the C–H (ACN)···I hydrogen bonds; (d) coordination geometries of Cu(I) in **CP3**; (e) formation of 2D layers with 1D double chains of (CuI) polymeric clusters connected by **3-PBI** linkers in the *bc*-plane; and (f) packing of 2D layers of **CP3**, and the layers are connected *via* N–H···O, C–H···O and C–H···I hydrogen bonding with a DMF molecule.

2.625(3), 2.774(3), 2.688(3), 2.622(3), 2.627(3) and 2.713(3) Å. The Cu···Cu distance between two adjacent Cu centres in this ladder-like cluster is 2.822(4) and 3.235(4) Å. Successive $(CuI)_n$ double chains are connected, along the *c*-axis, by **3-PBI** units to form a 2D layer (Fig. 1e). The 2D layers are further connected by the DMF *via* N–H···O (N···O, ∠N–H···O: 2.80(3) Å, 179°), C–H···O (C···O, ∠C–H···O: 3.27(3) Å, 169°) and C–H···I hydrogen bonds (C···I, ∠C–H···I: 3.79(2) Å, 116.4(3)°, Fig. 1f and inset).

Remarkably, the grinding of reddish-brown colored crystals of **CP1** and **CP2** using a mortar and pestle resulted in orange yellow materials **CP1G** and **CP2G**, respectively (Fig. 2a to d). In contrast, similar action on the crystals of **CP3** did not result in any change of color in **CP3G** (Fig. 2e and f). To understand the origin of such a difference in behavior, all the CPs and ground materials (CPxGs) were analyzed by PXRD, FT-IR and Raman spectroscopy. The PXRD analyses of the ground materials display similar powder patterns to their single crystals, indicating that no phase change occurred due to the applied mechanical stress and the material still maintained long range order (Fig. S3a–c, ESI†). According to findings by Kato and colleagues, the transition from crystalline to amorphous phases in coordination polymers (CPs) may be the primary cause of mechanochromism in CuX CPs.[60] However, in our case, this mechanism does not apply here as there was no structural change involved in grinding. The FT-IR and Raman spectroscopy of the ground material was performed to find out if any local distortion is involved. From the FT-IR analysis, **CP1** and **CP2** were found to lose the ACN present in their crystal lattice upon grinding. The characteristic C≡N stretching at 2247 cm^{-1} was found to be absent in both **CP1** and **CP2** after grinding (Fig. 3a and b). In addition, several other changes in IR were found, as some of the peaks shifted or weakened as shown in Fig. 3a and b and Table S5.† These results clearly indicate that grinding resulted in subtle changes in the environment around the Cu_nX_n cluster. Such grinding assisted solvent removal is not present in **CP3**. Also, it does not exhibit a distinguishable change in the local structure. The only difference from the linker FT-IR is the presence of the C=O stretching frequency of

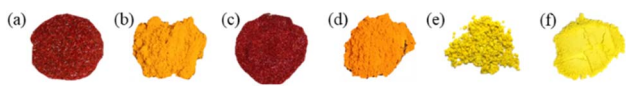

Fig. 2 Images of (a) **CP1**, (b) **CP1G**, (c) **CP2**, (d) **CP2G**, (e) **CP3** and (f) **CP3G**.

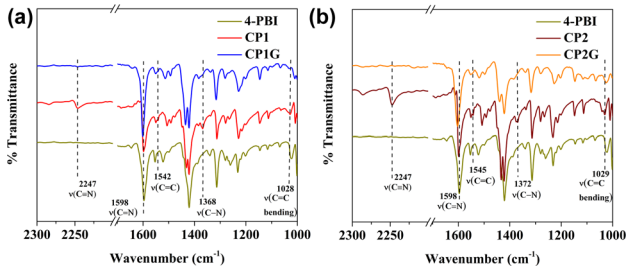

Fig. 3 FT-IR spectra of (a) 4-PBI, CP1 and CP1G and (b) 4-PBI, CP2 and CP2G.

the DMF molecule at 1671 cm^{-1}. All peaks present in the as-synthesized CP exactly match with those of the ground CP as shown in Fig. S4(a).†

The thermogravimetric analysis (TGA) of **CP1** and **CP2** showed an initial 10% weight loss within the range 120–222 °C for **CP1** (Fig. S5a, ESI†) and 120–170 °C for **CP2** (Fig. S5b, ESI†) due to the loss of ACN. On the other hand, the TGAs of **CP1G** and **CP2G** display no weight loss in the above temperature ranges, which further supports that grinding resulted in the loss of ACN. After the loss of ACN, the thermograms of the ground samples exhibit similar features to those of the parent CPs. Further, the heating of **CP1** and **CP2** at 150 °C for 2–3 hours also was found to result in ACN loss as conformed by FT-IR (Fig. S4b and c, ESI†). However, the heated samples were found to exhibit no colour change indicating that the solvent loss is not the sole cause of the chromism observed in the ground samples. Therefore, the phenomenon observed here can be termed mechanochromism as the change in colour occurred due to the application of mechanical force, not just due to the loss of solvent molecules. The TGA of **CP3** shows the loss of DMF (11%) in the range of 120 °C to 225 °C (Fig. S5c, ESI†).

The Raman spectra of **CP1** contain several weak peaks at 59, 64, 67, 76, 83 and 89 cm^{-1} as humps within a broad band, referring to the bending, rocking and wagging motions of I–Cu–N bonds. These types of motions are eventually found in the 50–130 cm^{-1} range as reported by Perruchas and co-workers.[66] Interestingly, all these bands in the Raman spectra of the ground material disappeared and two bands at 66 and 108 cm^{-1} appeared (Fig. 4a). The peak corresponding to Cu_2I_2 ring breathing also shifted from 125 cm^{-1} to 120 cm^{-1}, which is a direct indication of local structural distortion around the Cu centre in the crystal

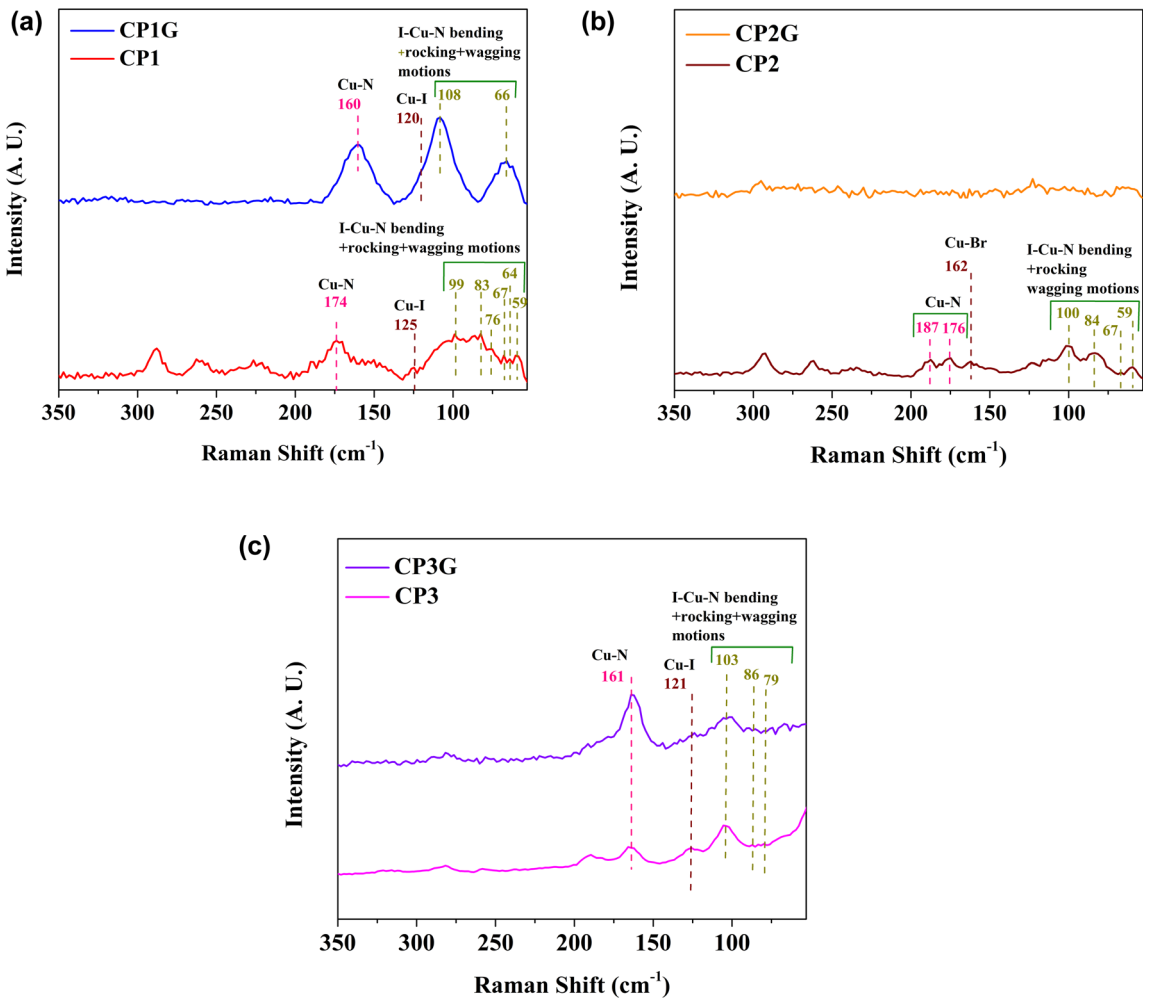

Fig. 4 Raman spectra of (a) CP1 and CP1G, (b) CP2 and CP2G, and (c) CP3 and CP3G.

lattice. Moreover, the Cu–N peak at 174 cm^{-1} shifted to 160 cm^{-1} upon grinding, which is also an indication of the mentioned change. In the case of **CP2**, the Raman spectra of the ground sample (**CP2G**) were found to be inactive as the s/n decreased (Fig. 4b). Further, the peaks in the as-synthesized CPs that arise from the internal motions of the cluster cores have either merged or became noticeably weakened in the ground CPs. This further indicates the grinding assisted local structural distortion might cause the dimeric Cu_2X_2 core to become more symmetric by altering the strength of several bonds that are associated with the SBUs. For **CP3**, the grinding had visually no effect on the local environment as all the significant peaks in the as-synthesized CP matched with those in the ground CP, **CP3G** (Fig. 4c). Therefore, it is evident from FT-IR and Raman of the CPs that the grinding created local perturbation in the cluster, which resulted in a change in color, probably due to the change in the HOMO–LUMO gap. Among the various studies on mechanochromic 1D CuI clusters, the primary distinction in photophysical properties arises from the flexibility of the Cu–I bonds, which enable different positioning of Cu(I) ions within the chain, thus altering the potential Cu···Cu interactions. In the case of **CP3**, the I^- ions are involved in μ_3-bridging and C–H···I interaction with the olefinic proton of the linker, making it more resistive towards any structural deformation that might be appearing due to mechanical grinding. As mentioned earlier, three such type of mechanochromic CPs containing ladder-like $(CuI)_n$ clusters have been reported by Amo-Ochoa and co-workers.[55–57] Among those, there are two 1D CPs containing monodentate ligands like 2-amino-4-chloropyrimidine and methyl isonicotinate, where the main propagation is controlled by the 1D cluster itself and the ligands remain only attached to the Cu(I) centres. No further strong coordination exists between two adjacent $(CuI)_n$ double chains, making the overall cluster somewhat flexible. However, the third one containing such a cluster was a mechanochromic 2D CP having an aminopyrazine linker to bind the adjacent clusters.

A diffuse reflectance spectroscopy (DRS) study was performed on the as-synthesized and ground samples to understand the differences in the absorption properties. In the case of as-synthesized **CP1** and **CP2**, a ligand centered absorption was observed at 295 nm along with a broad absorption band at 344–622 nm and 354–640 nm with absorption maxima at 453 nm and 514 nm for **CP1** and **CP2**, respectively (Fig. 5a and b).

For **CP1G** and **CP2G**, these broad bands were found to narrow down 344–570 nm and 354–606 nm with the absorption maxima of 419 and 432 nm, respectively. However, **CP3** exhibits nearly similar DRS before and after grinding (Fig. S6, ESI†).

Furthermore, the solid state photoluminescence (PL) spectra under 300 nm excitation were studied for **CP1** and **CP2**. Both **CP1** and **CP2** exhibited a broad emission band with maxima at 493 nm and 495 nm, respectively. The ground samples **CP1G** and **CP2G** display similar broad emissions at 514 and 517 nm, respectively, indicating red shifts of ~21–22 nm (Fig. 6a and b). However, **4-PBI** showed a slightly narrower but higher intensity emission band with $\lambda_{max} = 482$, while excited at 350 nm. The emission bands of CPs are likely to originate from several mixed electronic states, including ligand centred emission and charge transfer states like ^{3}MLCT and ^{3}XLCT states.[61] Both **CP1** and **CP2**, upon 420 nm excitation, exhibit weak emission bands at 650 nm and 652 nm, respectively. Upon grinding those were found to blue shift to 624 nm and 595 nm for **CP1** and **CP2**, respectively (Fig. 6a and b). These emission bands are likely to be halide-to-metal charge transfer (^{3}XMCT) bands as the possibility of a lower energy ^{3}CC state can be ruled out due to higher separation of Cu···Cu centres than the summation of van der Waal radii.[26,58] On the other hand, both **CP3** and **CP3G** showed a lower intensity ligand centred emission band at 518 nm at $\lambda_{ex} = 350$ nm (Fig. S7a, ESI†).

The excitation spectra of both **CP1** (Fig. S8a, ESI†) and **CP2** (Fig. S8b, ESI†) showed a 300 nm peak followed by a broad band from 350 nm to 600 nm with $\lambda_{max} = 490$ nm and 500 nm for **CP1** and **CP2**, respectively, reflecting the presence of different energy states. In the case of **CP3**, only one band in the excitation spectra (Fig. S8c, ESI†) with the maxima at 410 nm and a shoulder peak at 350 nm was observed. However, no characteristic emission was observed for both **CP3** and **CP3G** with $\lambda_{ex} = 400$ nm (Fig. S7b, ESI†).

The lifetime measurements of the emissive states were not successful despite several attempts. Thus, the possibility of Thermally Activated Delayed Fluorescence (TADF) could not be verified in these materials. However, for TADF, the destabilizing effect of Jahn–Teller distortion on the triplet excited state has to be reduced. Several studies have been reported to achieve such a stable triplet excited state by introducing a bulky linker or co-linker, *e.g.*, PPh_3, Phen, *etc.*,[67,68] while synthesizing $(CuX)_n$ cluster-based CPs or complexes. In our case, the linker **4-PBI** or **3-PBI** is not as bulky as those, which in turn rules out the possibility of TADF.

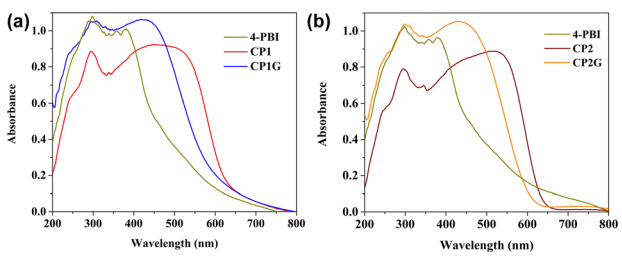

Fig. 5 Diffuse reflectance spectra (DRS) of (a) **4-PBI**, **CP1**, and **CP1G**, and (b) **4-PBI**, **CP2** and **CP2G**.

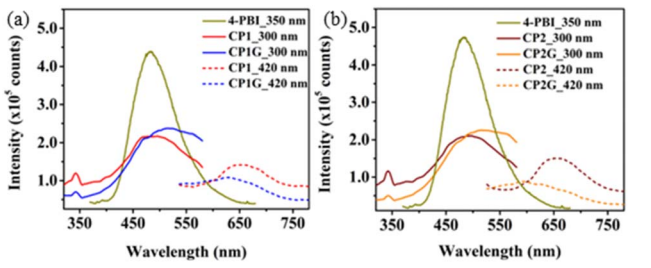

Fig. 6 Solid state PL spectra of (a) **4-PBI**, **CP1** and **CP1G** and (b) **4-PBI**, **CP2** and **CP2G** at different excitation wavelengths.

The CIE profiles of the CPs were also indicative of mechanochromic behavior.[69] As shown in Fig. S9(a) and (b),† both **CP1** and **CP2** were found to exhibit distinct shifts in CIE coordinates after grinding. As expected for **CP3** and **CP3G,** the coordinates almost overlapped (Fig. S9c, ESI†). Since **CP1** and **CP2** also show proper emission spectra while excited at 420 nm, the CIE profiles at those excitation wavelengths showed a similar distinct shift of coordinates from pristine to ground CPs (Fig. S9d and e, ESI†).

Combining FT-IR and Raman data shows a clear indication that the mechanical force affected the weak interactions assisted by solvents as well as cluster cores in all cases except **CP3**. The dimeric flexible cores in **CP1** and **CP2** are more vulnerable to external mechanical force, affecting the material's photophysical properties.

Conclusions

In conclusion, the crystal structures, mechanochromism and photo-physical properties of three Cu(I) halide coordination polymers with two isomeric linkers **4-PBI** and **3-PBI** have been explored. The two isomeric CPs containing Cu_2I_2 and Cu_2Br_2 rhomboidal clusters display changes in color and shifts in luminescence upon mechanical grinding. Significantly large Cu···Cu separation of **CP1** and **CP2** allowed the CPs to emit through ^{3}MLCT, ^{3}XLCT and ^{3}XMCT transitions, which upon mechanical perturbation showed distinguishable spectral shift, resulting in mechanochromic properties. **CP3**, on the other hand, remained non-mechanochromic due to its rigid layers, which are resistant to mechanical stress. PXRD, FT-IR and Raman analyses indicate the effect of mechanical grinding on the local environment around the cluster cores. From these studies, in general, it can be concluded that grinding resulted in the removal of solvent and generation of local defects around the cluster core in **CP1** and **CP2,** which in turn induced their non-phase transitional mechanochromic behavior.

Experimental

Materials and methods

4-Pyridinecarbaldehyde, 3-pyridinecarbaldehyde and malonic acid were purchased from Spectrochem, and *o*-phenylenediamine, polyphosphoric acid (PPA), pyridine, piperidine, diethylether (Et_2O), and 25% aq. ammonia solution were purchased from SRL Chemicals and were used without further purification. ^{1}H NMR spectra have been collected using a Bruker 400 Ultrashield spectrometer. HRMS was performed with an Agilent Mass Spectrometer in ESI (+ve) mode using a quadrupole time-of-flight (Q-TOF) mass analyser. PXRD patterns were recorded with a BRUKER-AXS-D8-ADVANCE diffractometer at room temperature (Cu target). FT-IR spectra were recorded with a PerkinElmer UATR Two Spectrometer. The Thermogravimetric Analysis (TGA) was performed using a PerkinElmer Pyris Diamond TG-DTA instrument with a heating rate of 10 °C min^{-1}. The diffuse reflectance spectra (DRS) of the solid samples were recorded with a Cary model 5000 UV-visible-NIR spectrophotometer. The reflectance data were transformed to absorbance by the Kubelka–Munk method.[70] The excitation spectra and solid-state photoluminescence spectra were collected with a Spex Fluorolog-3 (Model FL3-22) spectrofluorimeter. The Raman spectra were recorded with a Horiba LabRAM HR Evolution Raman Spectrometer (Model T64000) with an argon-krypton mixed ion gas laser excitation source with an excitation wavelength of 532 nm.

Synthetic procedures

Synthesis of the compound 4-PAA. 4-PAA was synthesized according to a previously reported procedure.[71] In a dry N_2 filled three-necked flask fitted with a stirrer, 4-pyridinecarbaldehyde (3.20 g, 30 mmol) and malonic acid (7.18 g, 70 mmol) were dissolved in 12 mL pyridine and 0.3 mL piperidine and the solution was heated to 90 °C for 1.5 h, and then at 130 °C for 3 h and the mixture was then worked up. To the suspension was added Et_2O (15 mL) and the white precipitate was filtered and washed with 10 mL Et_2O to obtain the product with a yield of 86%.

Synthesis of the compound 3-PAA. 3-PAA was synthesized using the exact same process as 4-PAA, by using 3-pyridinecarbaldehyde instead of 4-pyridinecarbaldehyde. Yield = 84%.

Synthesis of the compound 4-PBI. The ligand **4-PBI** was synthesized using a previously reported process.[72] 4-PAA (2.0 g, 13.4 mmol) and *o*-phenylenediamine (1.45 g, 13.4 mmol) were added to PPA and mixed thoroughly to make a pasty mass. The mixture was then heated slowly to 190–200 °C and stirred for 2–3 h; the mixture was allowed to cool to about 100 °C. Then, the viscous crude mixture was poured in a thin stream into a large volume of rapidly stirred cold water. The insoluble residue was collected by filtration, washed with water, and reslurried with aqueous ammonia to make the solution slightly basic (pH 8–9). Again, the solid residue was filtered and washed thoroughly with water until the residue part became base free. The product was dried under vacuum and recrystallized from a methanol–water mixture (2 : 1, v/v). A yellow crystalline material was isolated in good yield and characterized with ^{1}H NMR spectra (Fig. S1(a), ESI†) in DMSO-d_6. FT-IR (cm^{-1}): 3026, 1597, 1421, 1314, 955, 871, 805, 766, 744, 738, 688, 666, 602, 517, 503 and 440. HRMS (ESI): *m*/*z* calcd for $C_{14}H_{11}N_3$ $[M + H]^+$: 222.0987, found: 222.1028. m. p.: 232–234 °C. Yield = 75%.

Synthesis of the compound 3-PBI. 3-PBI was synthesized using the same process as **4-PBI** using 3-PAA instead of 4-PAA and characterized with ^{1}H NMR spectra (Fig. S1(b), ESI†) in DMSO-d_6. FT-IR (cm^{-1}): 3175, 1645, 1589, 1577, 1519, 1484, 1430, 1412, 1313, 1278, 1227, 1187, 1152, 1027, 962, 858, 799, 766, 741. HRMS (ESI): *m*/*z* calcd for $C_{14}H_{11}N_3$ $[M + H]^+$: 222.0987, found: 222.1029. m. p.: 253–254 °C. Yield = 72%.

General procedure for the synthesis of CPs

Each of 22.1 mg or 0.1 mmol of corresponding linker and 0.1 mmol of corresponding CuX salt was dissolved in 5 mL ACN solvent separately. The two solutions were mixed together and kept in a vial covered with perforated parafilm to allow slow evaporation of the solvent. After 4–5 days, crystals of CPs appeared.

Synthesis of CP1. The linker **4-PBI** and the metal salt CuI were used to obtain reddish brown block shaped crystals of **CP1** with a yield of 52%.

Synthesis of CP2. The linker **4-PBI** and the metal salt CuBr were used to obtain reddish brown block shaped crystals of **CP2** with 48% yield.

Synthesis of CP3. 11 mg (0.05 mmol) of **3-PBI** was dissolved in 5 mL of DMF and 19 mg (0.10 mmol) of CuI was dissolved in 8 mL ACN solvent separately. Next, a blank 2 mL ACN and DMF mixture was prepared in a 1 : 1 ratio. The blank solution was carefully layered over the DMF solution of **3-PBI** and the ACN solution of CuI was layered over the blank solution. After 6–7 days, yellow coloured crystals of **CP3** appeared in 48% yield.

Single crystal X-ray crystallography for analysing crystal structures

The single-crystal data of all the CPs were collected on a Bruker-D8 Venture X-ray diffractometer using graphite-monochromated Mo Kα radiation (λ = 0.71073 Å) at room temperature (300 K) and low temperature (120 K) by the hemisphere method. The structures were solved by direct methods and refined by least-squares methods on F^2 using SHELX-2014.[73] SADABS was applied for the adsorption correction of the diffractometer data. Non-hydrogen atoms were refined anisotropically and hydrogen atoms were fixed at calculated positions and refined using a riding model.

Data availability

The data supporting this article have been included as part of the ESI.† Crystallographic data for CP1, CP2 and CP3 have been deposited at the CCDC and can be obtained from [URL of data record, format **https://www.ccdc.cam.ac.uk/**].

Author contributions

The manuscript was written with the contributions of all authors. All authors have approved the final version of the manuscript.

Conflicts of interest

There are no conflicts to declare.

Acknowledgements

We acknowledge DST-SERB (CRG/2022/000606), New Delhi, India, for financial support. P. D. acknowledges IIT Kharagpur for research fellowship.

Notes and references

1 Y. Chen, H.-X. Li, D. Liu, L.-L. Liu, N.-Y. Li, H.-Y. Ye, Y. Zhang and J.-P. Lang, *Cryst. Growth Des.*, 2008, **8**, 3810–3816.
2 Z.-M. Hao, J. Wang and X.-M. Zhang, *CrystEngComm*, 2010, **12**, 1103–1109.
3 S. Hu, F.-Y. Yu, Y. Yan, Z.-F. Hao, L. Yu and M.-L. Tong, *Inorg. Chem. Commun.*, 2011, **14**, 622–625.
4 S.-L. Li, R. Zhang, J.-J. Hou and X.-M. Zhang, *Inorg. Chem. Commun.*, 2013, **32**, 12–17.
5 H.-B. Zhu and L. Liang, *J. Coord. Chem.*, 2015, **68**, 1306–1316.
6 C.-Y. Liu, X.-R. Chen, H.-X. Chen, Z. Niu, H. Hirao, P. Braunstein and J.-P. Lang, *J. Am. Chem. Soc.*, 2020, **142**, 6690–6697.
7 E. Cariati, E. Lucenti, C. Botta, U. Giovanella, D. Marinotto and S. Righetto, *Coord. Chem. Rev.*, 2016, **306**, 566–614.
8 Y. Zhang, M. Schulz, M. Wächtler, M. Karnahl and B. Dietzek, *Coord. Chem. Rev.*, 2018, **356**, 127–146.
9 A. Deák, C. Jobbágy, A. Demeter, L. Čelko, J. Cihlář, P. T. Szabó, P. Á. -Balogh, D. E. Crawford, D. Virieux and E. Colacino, *Dalton Trans.*, 2021, **50**, 13337–13344.
10 J. C. Deaton, S. C. Switalski, D. Y. Kondakov, R. H. Young, T. D. Pawlik, D. J. Giesen, S. B. Harkins, A. J. M. Miller, S. F. Mickenberg and J. C. Peters, *J. Am. Chem. Soc.*, 2010, **132**, 9499–9508.
11 Z. Liu, M. F. Qayyum, C. Wu, M. T. Whited, P. I. Djurovich, K. O. Hodgson, B. Hedman, E. I. Solomon and M. E. Thompson, *J. Am. Chem. Soc.*, 2011, **133**, 3700–3703.
12 X.-L. Chen, R. Yu, Q.-K. Zhang, L.-J. Zhou, X.-Y. Wu, Q. Zhang and C.-Z. Lu, *Chem. Mater.*, 2013, **25**, 3910–3920.
13 G. Kang, Y. Jeon, K. Y. Lee, J. Kim and T. H. Kim, *Cryst. Growth Des.*, 2015, **15**, 5183–5187.
14 S. Tunsrichon, K. Chainok, V. Promarak, P. Nalaoh, S. Youngme and J. Boonmak, *Inorg. Chem.*, 2022, **61**, 11734–11745.
15 A. Kobayashi and M. Kato, *Chem. Lett.*, 2017, **46**, 154–162.
16 J. López-Molina, C. Hernández-Rodríguez, R. Guerrero-Lemus, E. Cantelar, G. Lifante, M. Muñoz and P. Amo-Ochoa, *Dalton Trans.*, 2020, **49**, 4315–4322.
17 F. Hou, M. Powell, D. B. Dougherty, R. D. Sommer and P. A. Maggard, *Cryst. Growth Des.*, 2018, **18**, 5406–5416.
18 H.-X. Li, W. Zhao, H.-Y. Li, Z.-L. Xu, W.-X. Wanga and J.-P. Lang, *Chem. Commun.*, 2013, **49**, 4259–4261.
19 R. Peng, M. Li and D. Li, *Coord. Chem. Rev.*, 2010, **254**, 1–18.
20 E. Cariati, R. Ugo, F. Cariati, D. Roberto, N. Masciocchi, S. Galli and A. Sironi, *Adv. Mater.*, 2001, **13**, 1665–1668.
21 G. H. Li, Z. Shi, X. M. Liu, Z. M. Dai and S. H. Feng, *Inorg. Chem.*, 2004, **43**, 6884–6886.
22 S.-Q. Bai, J. Y. Kwang, L. L. Koh, D. J. Young and T. S. A. Hor, *Dalton Trans.*, 2010, **39**, 2631–2636.
23 L. Hou, W. J. Shi, Y. Y. Wang, H. H. Wang, L. Cui, P. X. Chen and Q. Z. Shi, *Inorg. Chem.*, 2011, **50**, 261–270.
24 W. Liu, Y. Fang, G. Z. Wei, S. J. Teat, K. Xiong, Z. Hu, W. P. Lustig and J. Li, *J. Am. Chem. Soc.*, 2015, **137**, 9400–9408.
25 K. Hassanein, P. Amo-Ochoa, C. J. Gómez-García, S. Delgado, O. Castillo, P. Ocón, J. I. Martínez, J. Perles and F. Zamora, *Inorg. Chem.*, 2015, **54**, 10738–10747.
26 H. Xiao, J. Zhou, X. Liu, H. P. Xiao, R. A. S. Ferreira, L. D. Carlos and L. S. Fu, *Dalton Trans.*, 2018, **47**, 3253–3257.
27 Y. Zhou, T. He, P. Yuan, J. Yin, S. Chen, L. Gutiérrez-Arzaluz, L. Wang, O. M. Bakr and O. F. Mohammed, *ACS Mater. Lett.*, 2023, **5**, 2002–2008.

28 J. Y. Lee, S. Y. Lee, W. Sim, K.-M. Park, J. Kim and S. S. Lee, *J. Am. Chem. Soc.*, 2008, **130**, 6902–6903.
29 Y. Zhao, M. Yu, C. Liu, S. Li, Z. Li, F. Jiang, L. Chen and M. Hong, *J. Mater. Chem. C*, 2021, **9**, 2890–2897.
30 L. I. Kursheva, O. N. Kataeva, D. B. Krivolapov, E. S. Batyeva and O. G. Sinyashin, *Heteroat. Chem.*, 2006, **17**, 542–546.
31 H. Tong, H. Li, Z. Zhou, Cidanpuchi, F. Wang and W. Liu, *New J. Chem.*, 2021, **45**, 10989–10996.
32 J. Troyano, F. Zamora and S. Delgado, *Chem. Soc. Rev.*, 2021, **50**, 4606–4628.
33 H. Park, E. Kwon, H. Chiang, H. Im, K. Y. Lee, J. Kim and T. H. Kim, *Inorg. Chem.*, 2017, **56**, 8287–8294.
34 A. Raghuvanshi, M. Knorr, L. Knauer, C. Strohmann, S. Boullanger, V. Moutarlier and L. Viau, *Inorg. Chem.*, 2019, **58**, 5753–5775.
35 J. Conesa-Egea, F. Zamora and P. Amo-Ochoa, *Coord. Chem. Rev.*, 2019, **381**, 65–78.
36 X.-C. Shan, F.-L. Jiang, H.-B. Zhang, X.-Y. Qian, L. Chen, M.-Y. Wu, S. A. Al-Thabaiti and M.-C. Hong, *Chem. Commun.*, 2013, **49**, 10227.
37 T. Wen, D.-X. Zhang, J. Liu, R. Lin and J. Zhang, *Chem. Commun.*, 2013, **49**, 5660.
38 L.-X. Hu, M. Gao, T. Wen, Y. Kang and S. Chen, *Inorg. Chem.*, 2017, **56**, 6507–6511.
39 H. D. Hardt and A. Z. Pierre, *Z. Anorg. Allg. Chem.*, 1973, **402**, 107–112.
40 N. C. Eddingsaas and K. S. Suslick, *J. Am. Chem. Soc.*, 2007, **129**, 6718–6719.
41 P. Xue, J. Ding, P. Wang and R. Lu, *J. Mater. Chem. C*, 2016, **4**, 6688–6706.
42 Z. Yang, Z. Chi, Z. Mao, Y. Zhang, S. Liu, J. Zhao, M. P. Aldred and Z. Chi, *Mater. Chem. Front.*, 2018, **2**, 861–890.
43 L. Huang, C. Qian and Z. Ma, *Chem.–Eur. J.*, 2020, **26**, 11914–11930.
44 B.-C. Tzeng, T.-Y. Chang and H.-S. Sheu, *Chem.–Eur. J.*, 2010, **16**, 9990–9993.
45 X. Zhang, Z. Chi, Y. Zhang, S. Liu and J. Xu, *J. Mater. Chem. C*, 2013, **1**, 3376–3390.
46 M. Krikorian, S. Liu and T. M. Swager, *J. Am. Chem. Soc.*, 2014, **136**, 2952–2955.
47 L. Liu, T. Wen, W.-Q. Fu, M. Liu, S. Chen and J. Zhang, *CrystEngComm*, 2016, **18**, 218–221.
48 X.-W. Chen, L.-H. He, P. Ju, J.-L. Chen, S.-J. Liu and H.-R. Wen, *J. Mater. Chem. C*, 2020, **8**, 16160–16167.
49 S. Perruchas, X. F. Le Goff, S. Maron, I. Maurin, F. Guillen, A. Garcia, T. Gacoin and J.-P. Boilot, *J. Am. Chem. Soc.*, 2010, **132**, 10967–10969.
50 X.-C. Shan, F.-L. Jiang, L. Chen, M.-Y. Wu, J. Pan, X.-Y. Wan and M.-C. Hong, *J. Mater. Chem. C*, 2013, **1**, 4339–4349.
51 X.-C. Shan, H.-B. Zhang, L. Chen, M.-Y. Wu, F.-L. Jiang and M.-C. Hong, *Cryst. Growth Des.*, 2013, **13**, 1377–1381.
52 Q. Benito, X. F. Le Goff, S. Maron, A. Fargues, A. Garcia, C. Martineau, F. Taulelle, S. Kahlal, T. Gacoin, J.-P. Boilot and S. Perruchas, *J. Am. Chem. Soc.*, 2014, **136**, 11311–11320.
53 Q. Benito, I. Maurin, T. Cheisson, G. Nocton, A. Fargues, A. Garcia, C. Martineau, T. Gacoin, J.-P. Boilot and S. Perruchas, *Chem.–Eur. J.*, 2015, **21**, 5892–5897.
54 K. Yang, S.-L. Li, F.-Q. Zhang and X.-M. Zhang, *Inorg. Chem.*, 2016, **55**, 7323–7325.
55 J. Conesa-Egea, J. Gallardo-Martínez, S. Delgado, J. I. Martínez, J. Gonzalez-Platas, V. Fernández-Moreira, U. R. Rodríguez-Mendoza, P. Ocón, F. Zamora and P. Amo-Ochoa, *Small*, 2017, **13**, 1700965.
56 J. Conesa-Egea, N. Nogal, J. I. Martínez, V. Fernández-Moreira, U. R. Rodríguez-Mendoza, J. González-Platas, C. J. Gómez-García, S. Delgado, F. Zamora and P. Amo-Ochoa, *Chem. Sci.*, 2018, **9**, 8000–8010.
57 J. López, M. Murillo, G. Lifante-Pedrola, E. Cantelar, J. Gonzalez-Platas, U. R. Rodríguez-Mendoza and P. Amo-Ochoa, *CrystEngComm*, 2022, **24**, 341–349.
58 M. S. Deshmukh, A. Yadav, R. Pant and R. Bhoomishankar, *Inorg. Chem.*, 2015, **54**, 1337–1345.
59 A. Schlachter, K. Tanner, R. Scheel, P.-L. Karsenti, C. Strohmann, M. Knorr and P. D. Harvey, *Inorg. Chem.*, 2021, **60**, 13528–13538.
60 A. Kobayashi, Y. Yoshida, M. Yoshida and M. Kato, *Chem.–Eur. J.*, 2018, **24**, 14750–14759.
61 E. Kwon, J. Kim, K. Y. Lee and T. H. Kim, *Inorg. Chem.*, 2017, **56**, 943–949.
62 M. Sarkar and K. Biradha, *Chem. Commun.*, 2005, 2229–2231.
63 S. Samai and K. Biradha, *Cryst. Growth Des.*, 2011, **11**, 5723–5732.
64 G. Mukherjee and K. Biradha, *Cryst. Growth Des.*, 2013, **13**, 4100–4109.
65 G. Mukherjee and K. Biradha, *CrystEngComm*, 2014, **16**, 4701–4705.
66 R. Utrera-Melero, B. Huitorel, M. Cordier, F. Massuyeau, J.-Y. Mevellec, N. Stephant, P. Deniard, C. Latouche, C. Martineau-Corcos and S. Perruchas, *J. Mater. Chem. C*, 2021, **9**, 7991–8001.
67 Z. A. Siddique, Y. Yamamoto, T. Ohno and K. Nozaki, *Inorg. Chem.*, 2003, **42**(20), 6366–6378.
68 C. E. McCusker and F. N. Castellano, *Inorg. Chem.*, 2013, **52**, 8114–8120.
69 E. H. H. Hasabeldaim, H. C. Swart and R. E. Kroon, *RSC Adv.*, 2023, **13**, 5353–5366.
70 M. L. Myrick, M. N. Simcock, M. Baranowski, H. Brooke, S. L. Morgan and J. N. Mccutcheon, *Appl. Spectrosc.*, 2011, **46**, 140–165.
71 E. Alcalde, I. Dinarés, L. Pérez-García and T. Roca, *Synthesis*, 1992, **04**, 395–398.
72 B.-C. Tzeng and J.-F. Lin, *Dalton Trans.*, 2019, **48**, 4046–4057.
73 G. M. Sheldrick, *SHELXL-2014, Program for the Solution and Refinement of Crystal Structures*, University of Göttingen and Bruker AXS, Karlsruhe, Germany, 2014.